

Entanglement enhancement in a modulated optomechanical system via squeezed vacuum field

Huan-Huan Cheng(程欢欢), Chen-Rui Yang(杨晨锐), Gao-Feng Jiao(焦高锋), Cheng-Hua Bai(白成华), and Shao-Xiong Wu(武少雄)

Citation: Chin. Phys. B, 2026, 35 (**4**): 040311. DOI: 10.1088/1674-1056/ae2d37
http://cpb.iphy.ac.cn; http://iopscience.iop.org/cpb

What follows is a list of articles you may be interested in

Enhancing entanglement and steering in a hybrid atom-optomechanical system via Duffing nonlinearity

Ling-Hui Dong(董凌晖), Xiao-Jie Wu(武晓捷), Cheng-Hua Bai(白成华), and Shao-Xiong Wu(武少雄)
Chin. Phys. B, 2025, 34 (**2**): 020304. DOI: 10.1088/1674-1056/ad9ba2

Nonlinear enhanced mass sensor based on optomechanical system

Xin-Xin Man(满鑫鑫), Jing Sun(孙静), Wen-Zhao Zhang(张闻钊), Lijuan Luo(罗丽娟), and Guangri Jin(金光日)
Chin. Phys. B, 2024, 33 (**12**): 120303. DOI: 10.1088/1674-1056/ad84cf

Nonreciprocal mechanical entanglement in a spinning optomechanical system

Shan-Shan Chen(陈珊珊), Jing-Jing Zhang(张京京), Jia-Neng Li(李嘉能), Na-Na Zhang(张娜娜), Yong-Rui Guo(郭永瑞), and Huan Yang(杨桓)
Chin. Phys. B, 2024, 33 (**11**): 110305. DOI: 10.1088/1674-1056/ad72e1

Nonlinearly induced entanglement in dissipatively coupled optomechanical system

Wen-Quan Yang(杨文全), Xuan Leng(冷轩), Jiong Cheng(程泂), and Wen-Zhao Zhang(张闻钊)
Chin. Phys. B, 2024, 33 (**6**): 060313. DOI: 10.1088/1674-1056/ad3dd6

Direct measurement of two-qubit phononic entangled states via optomechanical interactions

A-Peng Liu(刘阿鹏), Liu-Yong Cheng(程留永), Qi Guo(郭奇), Shi-Lei Su(苏石磊), Hong-Fu Wang(王洪福), and Shou Zhang(张寿)
Chin. Phys. B, 2022, 31 (**8**): 080307. DOI: 10.1088/1674-1056/ac5d2f

---

Entanglement enhancement in a modulated optomechanical system via squeezed vacuum field

Huan-Huan Cheng(程欢欢), Chen-Rui Yang(杨晨锐), Gao-Feng Jiao(焦高锋), Cheng-Hua Bai(白成华), and Shao-Xiong Wu(武少雄)[†]

School of Semiconductor and Physics, North University of China, Taiyuan 030051, *China*

(Received 27 October 2025; revised manuscript received 11 December 2025; accepted manuscript online 16 December 2025)

We present a double-cavity optomechanical system with a mechanical oscillator, which is jointly driven by an amplitude-modulated laser field and a weak squeezed vacuum field, aiming to explore quantum entanglement effects under the unresolved-sideband regime. Within our proposed scheme, it is possible not only to surpass the limit of maximum steady-state entanglement ln2 for bipartite entanglement, achieving strong entanglement, but also to significantly enhance tripartite entanglement and improve the system's robustness against thermal noise. Meanwhile, the introduction of the squeezed vacuum field plays a crucial role in entanglement control, enabling not only a several-fold enhancement of entanglement but also continuous and precise manipulation of its strength within specific ranges. The suggested method demonstrates exceptional flexibility and adaptability under a wide range of operating conditions, offering a new pathway for theoretical and experimental investigations of strong bipartite entanglement and tripartite entanglement.

Keywords: optomechanical system, quantum entanglement, pump modulation, squeezed vacuum field

PACS: 03.65.Ud, 03.67.Mn, 42.50.–p

DOI: 10.1088/1674-1056/ae2d37 **CSTR:** 32038.14.CPB.ae2d37

1. Introduction

Cavity optomechanical systems are complex hybrid systems characterized by the coupling interaction between the cavity field and a mechanical oscillator.[1–3] They not only offer a crucial platform for exploring the boundary where the classical world interacts with the quantum realm but also hold immense significance for the investigation of nonclassical and nonlinear phenomena.[4–7] With the rapid development of high-precision instrument technology, optical microcavities are continuously shrinking in size while experiencing significant improvements in quality factors. In various meticulously designed systems, the interaction between photons and matter mediated by radiation pressure has led to a multitude of novel quantum effects,[8] such as quantum entanglement,[9–17] Einstein–Podolsky–Rosen (EPR) steering,[18–21] mechanical squeezing,[22–26] photon blockade,[27–32] nonreciprocal transmission,[33,34] and quantum synchronization.[35–38] These phenomena hold theoretical significance and demonstrate great potential for practical applications.

Among various quantum phenomena, quantum entanglement has become a major focus of research. Quantum entanglement can generally be classified into bipartite entanglement and multipartite entanglement. Bipartite entanglement takes various forms, such as optomechanical entanglement, photon–photon entanglement, photon–microwave entanglement, photon–atom entanglement, and others.[39–42] Our proposal aims to investigate optomechanical entanglement, which denotes a unique quantum state that arises between photons (light fields) and mechanical oscillators (tiny physical vibration systems) within the framework of quantum optics and quantum mechanics. In this entangled state, the photon and the mechanical oscillator are intrinsically linked to form a unified system, allowing them to influence each other despite being spatially separated. The concept of entanglement stems from debates on the completeness of quantum mechanics. In 1935, Einstein, Podolsky, and Rosen proposed the EPR paradox,[10] which marked the emergence of quantum entanglement as a cornerstone for quantum information processing. Subsequently, Schrödinger coined the concept of quantum entanglement to describe the relationship between two particles in the EPR thought experiment and to consider how to steer the entanglement.[11] Meanwhile, multipartite quantum entanglement serves as a core resource for examining the essence of quantum non-locality and quantum correlations. Compared to bipartite entanglement, tripartite and higher-order multipartite entanglements exhibit richer structural characteristics and stronger information processing capabilities.[43–47] Our research primarily focuses on tripartite entanglement within the framework of continuous variables, aiming to construct stable three-mode entangled states through coordinated regulation between two optical modes and one mechanical mode. This enables us to investigate the quantification rules, dynamic evolution characteristics, and robustness against external noise of tripartite entanglement. To date, entanglement between mi-

[†]Corresponding author. E-mail: sxwu@nuc.edu.cn

© 2026 Chinese Physical Society and IOP Publishing Ltd. All rights, including for text and data mining, AI training, and similar technologies, are reserved.

croscopic particles has been achieved in various systems, such as optomechanical and magnomechanical cavities.[48–51]

However, quantum states such as entanglement are relatively fragile. External disturbances, such as thermal noise, can cause decoherence of quantum states, ultimately leading to the loss of nonclassical features of the quantum system. Specifically, thermal noise increases the uncertainty in both optical and mechanical modes, limits the achievable degree of squeezing, and makes it difficult to maintain quantum correlations between subsystems, severely degrading both the stability and observability of entanglement. To alleviate the detrimental effects of thermal noise, various strategies have been proposed, including the introduction of atomic ensembles,[9,52] squeezed vacuum fields,[20] optical parametric amplifiers,[25,53,54] auxiliary optical cavities,[55,56] and periodically modulated laser fields.[57–59] Specifically, Zhang *et al*. investigated steady-state mechanical squeezing and optomechanical bipartite entanglement in a cavity driven by a laser with a periodically modulated amplitude, comparing cases with and without an auxiliary cavity.[57] They found that in the resolved-sideband regime, mechanical squeezing can exceed the 3-dB limit, and bipartite entanglement is significantly enhanced. Meanwhile, Wu *et al*. explored how to enhance quantum entanglement and EPR steering in an optomechanical system coupled to a squeezed vacuum field, taking into account the displacement of detuning induced by the mechanical mode.[20] In this work, by combining a periodically amplitude-modulated driving laser with a squeezed vacuum field, we not only examine optomechanical bipartite entanglement but also innovatively investigate the influence of the squeezed vacuum field on tripartite entanglement. Here, we focus specifically on the role of the squeezed vacuum field. In quantum optics, the squeezed vacuum field is a type of nonclassical optical field that surpasses the classical noise limit. Its essential feature lies in the directional redistribution of quantum noise through nonlinear optical processes. It achieves this by squeezing fluctuations in one quadrature component (e.g., momentum or position) to fall below the standard quantum limit (i.e., 1/2) while correspondingly enhancing noise in the conjugate quadrature to satisfy the uncertainty principle. This "noise redistribution" mechanism provides a crucial resource for the generation and enhancement of entangled states. Meanwhile, this noise reduction effect can be effectively transmitted through the interactions among subsystems, thereby maximizing the entanglement effect. Furthermore, by combining the dynamic tunability of the squeezed vacuum field with the adjustable coupling in the dual-cavity system, the strength of the entangled state can be switched on demand, allowing for flexible and precise control.

In traditional dual-cavity optomechanical systems, increasing quantum entanglement suffers from a plateau effect, making it difficult to surpass the threshold of maximum steady-state entanglement, $\ln 2$.[57] In this work, the coupled optomechanical system is driven by an amplitude-modulated laser field and a squeezed vacuum field. It is found that the bipartite entanglement thus produced can easily exceed the limit of steady-state entanglement, $\ln 2$. Compared to the case without the squeezed vacuum field, the maximum entanglement is increased to 2.76 times its original value. Moreover, tripartite entanglement is also significantly strengthened, and both exhibit strong robustness. Furthermore, by tuning the parameters of the squeezed vacuum field and the intercavity coupling, the degree of entanglement can be continuously adjusted and precisely controlled within a certain range. This approach offers a novel perspective for the study of bipartite and tripartite entanglement.

The organization of this paper is as follows. In Section 2, the system model and the linearized Hamiltonian are introduced. In Section 3, we investigate the dynamic behavior of the system and formulate the dynamical evolution equations for the system operators. In Section 4, we explore bipartite and tripartite entanglement in the optomechanical system while separately verifying their robustness. The conclusions are summarized at the end.

2. Model and Hamiltonian

The modulated optomechanical system is depicted in Fig. 1, in which two coupled whispering-gallery-mode optical cavities (one of which is coupled to a mechanical resonator) are driven by an external coherent driving laser with a time-dependent amplitude $E(t)$ and frequency ω_0. A weak squeezed vacuum field is also applied to the driving laser. The system Hamiltonian can be written as (in units of $\hbar = 1$)

$$\begin{aligned} H \;=\; & \omega_1 a_1^\dagger a_1 + \omega_2 a_2^\dagger a_2 + \frac{\omega_m}{2}(p^2+q^2) + J(a_1^\dagger a_2 + a_1 a_2^\dagger) \\ & - G_0 a_1^\dagger a_1 q + \mathrm{i}[E(t) a_1^\dagger \mathrm{e}^{-\mathrm{i}\omega_0 t} - E^*(t) a_1 \mathrm{e}^{\mathrm{i}\omega_0 t}]. \end{aligned} \tag{1}$$

Here, $a_1(a_1^\dagger)$ and $a_2(a_2^\dagger)$ denote the annihilation (creation) operators for the two cavity modes with frequencies ω_1, ω_2 and decay rates κ_1, κ_2, respectively; q and p represent the dimensionless position and momentum operators of the mechanical oscillator m, which satisfy the standard canonical commutation relation $[q,p] = \mathrm{i}$. The single-photon coupling strength is denoted by G_0, and the cavity–cavity coupling strength is represented by J. In the rotating frame at the laser frequency ω_0, the Hamiltonian (1) takes the form

$$\begin{aligned} H' \;=\; & \delta_1 a_1^\dagger a_1 + \delta_2 a_2^\dagger a_2 + \frac{\omega_m}{2}(p^2+q^2) - G_0 a_1^\dagger a_1 q \\ & + J(a_1^\dagger a_2 + a_1 a_2^\dagger) + \mathrm{i}[E(t) a_1^\dagger - E^*(t) a_1], \end{aligned} \tag{2}$$

where $\delta_1 = \omega_1 - \omega_0$ and $\delta_2 = \omega_2 - \omega_0$ represent the detunings of the two cavities with respect to the driving laser, respectively.

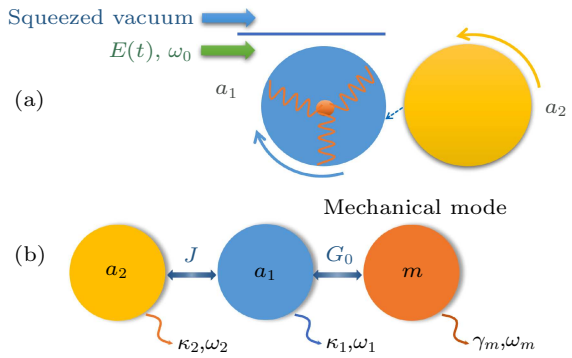


Fig. 1. Schematic diagram of the optomechanical system. (a) The cavity a_1 is coupled to a mechanical oscillator m and another cavity a_2. Cavity a_1 is driven by an external coherent laser with a periodically modulated amplitude $E(t)$ and a weak squeezed vacuum field. (b) The cavities a_1 (with frequency ω_1 and decay rate κ_1) and a_2 (with frequency ω_2 and decay rate κ_2) are coupled with a coupling strength J. Additionally, the cavity a_1 is coupled to a mechanical oscillator m (with frequency ω_m and damping rate γ_m) via a coupling strength G_0.

In addition to the coherent dynamics, the system is inevitably affected by the environment. If we take into account the mechanical damping and cavity decays, the dynamics of the system can be described by the nonlinear quantum Langevin equations (QLEs)

$$\begin{aligned}
\dot{q} &= \omega_m p,\\
\dot{p} &= -\omega_m q - \frac{\gamma_m}{2}p + G_0 a_1^\dagger a_1 + \xi(t),\\
\dot{a}_1 &= -\left(\frac{\kappa_1}{2} + \mathrm{i}\delta_1\right)a_1 + \mathrm{i}G_0 a_1 q - \mathrm{i}J a_2 + E + \sqrt{\kappa_1}a_1^{\mathrm{in}},\\
\dot{a}_2 &= -\left(\frac{\kappa_2}{2} + \mathrm{i}\delta_2\right)a_2 - \mathrm{i}J a_1 + \sqrt{\kappa_2}a_2^{\mathrm{in}},
\end{aligned} \tag{3}$$

where a_1^{in} and a_2^{in} are zero-mean input noise operators of the two cavities, characterized by the following correlation functions:

$$\begin{aligned}
\langle {a_1}^{\mathrm{in}\dagger}(t)a_1^{\mathrm{in}}(t')\rangle &= N\delta(t-t'),\\
\langle {a_1}^{\mathrm{in}}(t)a_1^{\mathrm{in}}(t')\rangle &= M\delta(t-t'),\\
\langle {a_2}^{\mathrm{in}\dagger}(t)a_2^{\mathrm{in}}(t')\rangle &= n_{\mathrm{th}}\delta(t-t').
\end{aligned} \tag{4}$$

The coefficients $N = \sinh^2 r$ and $M = \mathrm{e}^{\mathrm{i}\theta}\sinh r\cosh r$ denote the features of the squeezed vacuum field with squeezing parameter r and reference phase θ, and $n_{\mathrm{th}} = [\exp(\hbar\omega_2/k_{\mathrm{B}}T) - 1]^{-1}$ denotes the average photon number at the thermal environmental temperature T, with k_{B} being the Boltzmann constant. $\xi(t)$ is a zero-mean Brownian motion noise operator. For a high-quality mechanical oscillator satisfying $Q = \omega_m/\gamma_m \gg 1$, the correlation function of ξ can be described as $\langle\xi(t)\xi(t') + \xi(t')\xi(t)\rangle/2 \simeq \frac{\gamma_m}{2}(2n_m+1)\delta(t-t')$ with the mean thermal phonon number $n_m = [\exp(\hbar\omega_m/k_{\mathrm{B}}T) - 1]^{-1}$.

The QLEs in Eq. (3) are nonlinear inhomogeneous differential equations, which are generally challenging to solve directly. However, under the strong driving condition, the equations can be solved through a standard linearization technique. Specifically, the cavity mode and mechanical mode can be expressed as the sum of the classical mean value and the quantum fluctuation operator, i.e., $O = \langle O(t)\rangle + \delta O, (O = a_1, a_2, q, p)$. The differential equations for the classical mean values are as follows:

$$\begin{aligned}
\langle\dot{q}(t)\rangle &= \omega_m\langle p(t)\rangle,\\
\langle\dot{p}(t)\rangle &= -\omega_m\langle q(t)\rangle - \frac{\gamma_m}{2}\langle p(t)\rangle + G_0|\langle a_1(t)\rangle|^2,\\
\langle\dot{a}_1(t)\rangle &= -\left(\frac{\kappa_1}{2} + \mathrm{i}\delta_1\right)\langle a_1(t)\rangle + \mathrm{i}G_0\langle a_1(t)\rangle\langle q(t)\rangle\\
&\quad - \mathrm{i}J\langle a_2(t)\rangle + E(t),\\
\langle\dot{a}_2(t)\rangle &= -\left(\frac{\kappa_2}{2} + \mathrm{i}\delta_2\right)\langle a_2(t)\rangle - \mathrm{i}J\langle a_1(t)\rangle.
\end{aligned} \tag{5}$$

The linearized QLEs governing the quantum fluctuation operators are as follows:

$$\begin{aligned}
\delta\dot{q} &= \omega_m\delta p,\\
\delta\dot{p} &= -\omega_m\delta q - \frac{\gamma_m}{2}\delta p + G_0\langle a_1(t)\rangle^*\delta a_1 + G_0\langle a_1(t)\rangle\delta a_1^\dagger\\
&\quad + \xi(t),\\
\delta\dot{a}_1 &= -\left(\frac{\kappa_1}{2} + \mathrm{i}\delta_1\right)\delta a_1 + \mathrm{i}G_0\langle a_1(t)\rangle\delta q + \mathrm{i}G_0\langle q(t)\rangle\delta a_1\\
&\quad - \mathrm{i}J\delta a_2 + \sqrt{\kappa_1}a_1^{\mathrm{in}}(t),\\
\delta\dot{a}_2 &= -\left(\frac{\kappa_2}{2} + \mathrm{i}\delta_2\right)\delta a_2 - \mathrm{i}J\delta a_1 + \sqrt{\kappa_2}a_2^{\mathrm{in}}(t).
\end{aligned} \tag{6}$$

The linearized system Hamiltonian associated with the quantum fluctuation operators can be derived as follows:

$$\begin{aligned}
H_{\mathrm{lin}} &= [\delta_1 - G_0\langle q(t)\rangle]\delta {a_1}^\dagger\delta a_1 + \delta_2\delta {a_2}^\dagger\delta a_2\\
&\quad + \frac{\omega_m}{2}(\delta q^2 + \delta p^2) + J(\delta {a_2}^\dagger\delta a_1 + \delta a_2\delta {a_1}^\dagger)\\
&\quad - G_0[\langle a_1(t)\rangle^*\delta a_1 + \langle a_1(t)\rangle\delta {a_1}^\dagger]\delta q.
\end{aligned} \tag{7}$$

3. Dynamics of the system

The time evolution of the mean value operators captures the classical dynamics of the system. When the system is far from regions of instability or multistability, the optomechanical interaction can be treated as a perturbation. According to Floquet theory, the asymptotic solutions of the first moments will exhibit the same periodicity as the behavior of amplitude modulation, i.e., $\langle O(t+\tau)\rangle = \langle O(t)\rangle$. Therefore, we can perform a double expansion (Fourier and perturbation expansions) on the mean value operators:

$$\langle O(t)\rangle = \sum_{l=0}^{\infty}\sum_{n=-\infty}^{\infty} O_{n,l}\,\mathrm{e}^{\mathrm{i}n\Omega t}G_0^l, \tag{8}$$

where the indices n and l are integers, and $\Omega = 2\pi/\tau$ denotes the modulation frequency. The periodic amplitude driving $E(t)$ can also be expanded as a Fourier series

$$E(t) = \sum_{n=-\infty}^{\infty} E_n\,\mathrm{e}^{-\mathrm{i}n\Omega t}. \tag{9}$$

Substituting Eqs. (8) and (9) into Eq. (5), we obtain recursive formulas for the time-independent coefficients $O_{n,l}$:

$$\begin{aligned} q_{n,0} &= 0,\ p_{n,0} = 0, \\ a_1^{n,0} &= \frac{E_{-n}\left[\frac{\kappa_2}{2} + \mathrm{i}(n\Omega + \delta_2)\right]}{\left[\frac{\kappa_1}{2} + \mathrm{i}(n\Omega + \delta_1)\right]\left[\frac{\kappa_2}{2} + \mathrm{i}(n\Omega + \delta_2)\right] + J^2}, \\ a_2^{n,0} &= \frac{JE_{-n}}{\mathrm{i}\left[\frac{\kappa_1}{2} + \mathrm{i}(n\Omega + \delta_1)\right]\left[\frac{\kappa_2}{2} + \mathrm{i}(n\Omega + \delta_2)\right] + \mathrm{i}J^2}. \end{aligned} \tag{10}$$

The resulting equations correspond to the case where $l = 0$. For $l \geq 1$, the solutions are given by

$$\begin{aligned} p_{n,l} &= \frac{\mathrm{i}n\Omega\omega_m}{q_{n,l}}, \\ q_{n,l} &= \omega_m \sum_{l'=0}^{l-1} \sum_{n'=-\infty}^{\infty} \frac{a_1^{n',l'*} a_1^{n'+n,l-l'-1}}{\omega_m^2 - n^2\Omega^2 + \frac{\mathrm{i}n\Omega\gamma_m}{2}}, \\ a_1^{n,l} &= \sum_{l'=0}^{l-1} \sum_{n'=-\infty}^{\infty} \frac{\mathrm{i}\left[\frac{\kappa_2}{2} + \mathrm{i}(n\Omega + \delta_2)\right] a_1^{n',l'} q_{n-n',l-l'-1}}{\left[\frac{\kappa_1}{2} + \mathrm{i}(n\Omega + \delta_1)\right]\left[\frac{\kappa_2}{2} + \mathrm{i}(n\Omega + \delta_2)\right] + J^2}, \\ a_2^{n,l} &= \sum_{l'=0}^{l-1} \sum_{n'=-\infty}^{\infty} \frac{J a_1^{n',l'} q_{n-n',l-l'-1}}{\left[\frac{\kappa_1}{2} + \mathrm{i}(n\Omega + \delta_1)\right]\left[\frac{\kappa_2}{2} + \mathrm{i}(n\Omega + \delta_2)\right] + J^2}. \end{aligned} \tag{11}$$

To obtain a relatively accurate analytical solution, we truncate the above series at $l \leq 6$ and $|n| \leq 5$, and truncate the series of the modulation amplitude $E(t)$ at $|n| \leq 1$. For our experimental conditions,[60–64] reasonable experimental parameters are assumed as follows. The frequency of the mechanical oscillator m is set to $\omega_m = 2\pi \times 23.4$ MHz, with a corresponding quality factor of $\mathcal{Q} = 10^3$. Compared to high quality factors, the one we have chosen is easier to achieve experimentally. The main amplitude of the driving light $E_0 = \sqrt{\kappa P_0/\hbar\omega} = 1.5 \times 10^5 \omega_m$ with $\kappa = 5\kappa_1$, and the corresponding power $P_0 \simeq 3.38$ mW. For optical cavities, the frequencies of a_1 and a_2 are both set to $\omega_{1,2} = 2\pi \times 193.4$ THz, with quality factors of $\mathcal{Q}_1 = 2 \times 10^6$ and $\mathcal{Q}_2 = 8 \times 10^7$, respectively. By precisely adjusting the distance between the two cavities, their coupling strength can be experimentally regulated. Furthermore, squeezed vacuum fields have been experimentally applied for years;[65,66] they can be generated by a flux-driven Josephson parametric amplifier, and their mature experimental technology provides strong support for the experimental implementation of our proposal. The above analysis has advanced our scheme from theory to practice.

Subsequently, we analyze the time-evolution behavior of the phase space trajectories for the mechanical modes $\langle q(t)\rangle$ and $\langle p(t)\rangle$ in Fig. 2(a). It can be observed that the evolutionary behavior of the mechanical mode exhibits periodicity. As time progresses, the numerical results align with the analytical predictions, with both converging to a limit cycle. This confirms that the evolutionary period of the mechanical mode is consistent with the modulation period τ. Figures 2(b) and 2(c) respectively show the asymptotic behaviors of the real and imaginary parts of $\langle a_1(t)\rangle$ and $\langle a_2(t)\rangle$ over time. After approximately 60 modulation periods, the approximate analytical solution agrees closely with the exact numerical solution, further verifying the accuracy of the analytical approach.

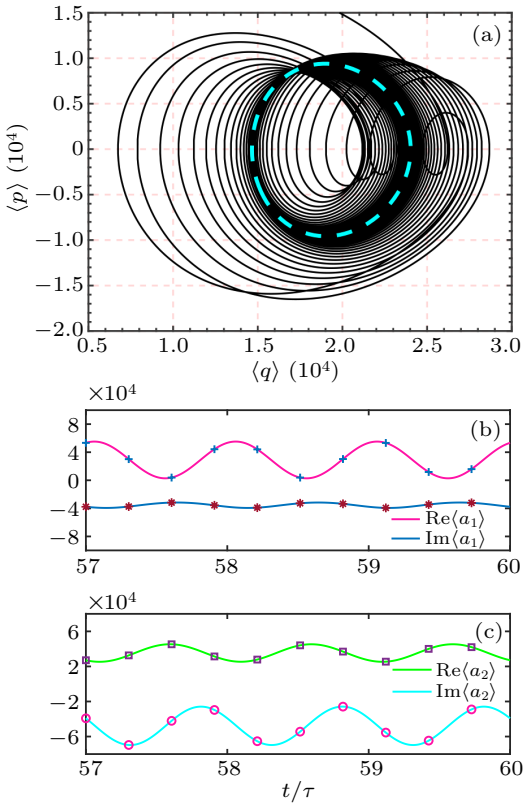


Fig. 2. The phase-space trajectories of the first moments $\langle q(t)\rangle$ and $\langle p(t)\rangle$ (a) over the time interval $[0, 60\tau]$; the cyan dashed line and black solid line represent the approximate analytical and exact numerical results, respectively. The time evolution of the real and imaginary parts of the first moments $\langle a_1(t)\rangle$ (b) and $\langle a_2(t)\rangle$ (c) during the three modulation periods $[57\tau, 60\tau]$; the marker symbols and solid lines correspond to the approximate analytical and exact numerical results, respectively. The system parameters are chosen as follows: $\delta_1/\omega_m = 1$, $G_0/\omega_m = 8 \times 10^{-6}$, $\Omega/\omega_m = 2$, $\kappa_1/\omega_m = 4$, $\tau = 2\pi/\Omega$, $\gamma_m/\omega_m = 10^{-3}$, $\kappa_2/\omega_m = 0.1$, $\delta_2/\omega_m = -1$, $J/\omega_m = 1.3$, $E_0/\omega_m = 1.5 \times 10^5$, and $E_{\pm 1}/\omega_m = 3 \times 10^4$.

Having obtained the time evolution of the mean values, we proceed to investigate the dynamics of quantum fluctuations. To this end, we introduce the quadrature operators of the cavity mode along with the corresponding Hermitian input noise operators:

$$\begin{aligned} \delta x_1 &= \frac{\delta a_1 + \delta a_1^\dagger}{\sqrt{2}}, \quad \delta y_1 = \frac{\delta a_1 - \delta a_1^\dagger}{\mathrm{i}\sqrt{2}}, \\ \delta x_2 &= \frac{\delta a_2 + \delta a_2^\dagger}{\sqrt{2}}, \quad \delta y_2 = \frac{\delta a_2 - \delta a_2^\dagger}{\mathrm{i}\sqrt{2}}, \\ x_1^{\mathrm{in}} &= \frac{a_1^{\mathrm{in}} + a_1^{\mathrm{in}\dagger}}{\sqrt{2}}, \quad y_1^{\mathrm{in}} = \frac{a_1^{\mathrm{in}} - a_1^{\mathrm{in}\dagger}}{\mathrm{i}\sqrt{2}}, \\ x_2^{\mathrm{in}} &= \frac{a_2^{\mathrm{in}} + a_2^{\mathrm{in}\dagger}}{\sqrt{2}}, \quad y_2^{\mathrm{in}} = \frac{a_2^{\mathrm{in}} - a_2^{\mathrm{in}\dagger}}{\mathrm{i}\sqrt{2}}. \end{aligned} \tag{12}$$

The quadrature operators of the quantum fluctuations and the corresponding noise operators can be reexpressed as column vectors:

$$\begin{aligned} \mathcal{U}(t) &= [\delta q, \delta p, \delta x_1, \delta y_1, \delta x_2, \delta y_2]^{\mathrm{T}}, \\ \mathcal{N}(t) &= [0, \xi(t), \sqrt{\kappa_1} x_1^{\mathrm{in}}(t), \sqrt{\kappa_1} y_1^{\mathrm{in}}(t), \sqrt{\kappa_2} x_2^{\mathrm{in}}(t), \sqrt{\kappa_2} y_2^{\mathrm{in}}(t)]^{\mathrm{T}}. \end{aligned} \tag{13}$$

Then, the linearized QLEs (6) of the fluctuations can also be rewritten in a more succinct form

$$\frac{\mathrm{d}\mathcal{U}(t)}{\mathrm{d}t}=\mathcal{R}(t)\mathcal{U}(t)+\mathcal{N}(t), \tag{14}$$

where the time-dependent 6×6 drift matrix $\mathcal{R}(t)$ has the following form:

$$\mathcal{R}(t)=\begin{pmatrix} 0 & \omega_m & 0 & 0 & 0 & 0 \\ -\omega_m & -\frac{\gamma_m}{2} & G_x(t) & G_y(t) & 0 & 0 \\ -G_y(t) & 0 & -\frac{\kappa_1}{2} & \Delta_1(t) & 0 & J \\ G_x(t) & 0 & -\Delta_1(t) & -\frac{\kappa_1}{2} & -J & 0 \\ 0 & 0 & 0 & J & -\frac{\kappa_2}{2} & \delta_2 \\ 0 & 0 & -J & 0 & -\delta_2 & -\frac{\kappa_2}{2} \end{pmatrix}$$

with $\Delta_1(t)=\delta_1-G_0\langle q(t)\rangle$, $G(t)=\sqrt{2}G_0\langle a_1(t)\rangle$. The coefficients G_x and G_y are the real and imaginary parts of $G(t)$, respectively. Due to the linearization process of quantum fluctuations and the intrinsically Gaussian nature of noise, the time evolution of the fluctuations can be completely characterized by a 6×6 covariance matrix (CM) $\mathcal{V}(t)$, with its elements defined by the following equation:

$$\mathcal{V}_{k,l}=\langle \mathcal{R}_k(t)\mathcal{R}_l(t)+\mathcal{R}_l(t)\mathcal{R}_k(t)\rangle/2. \tag{15}$$

The motion equation for the CM can be derived from Eqs. (14) and (15) and is governed by

$$\frac{\mathrm{d}\mathcal{V}}{\mathrm{d}t}=\mathcal{R}(t)\mathcal{V}(t)+\mathcal{V}(t)\mathcal{R}(t)^{\mathrm{T}}+\mathcal{D}, \tag{16}$$

where the noise diffusion matrix $\mathcal{D}$ with element $\mathcal{D}_{kl}\delta(t-t')=\langle n_k(t)n_l(t')+n_l(t')n_k(t)\rangle/2$ can be written as $\mathcal{D}=\mathcal{D}_1\oplus\mathcal{D}_2\oplus\mathcal{D}_3$ with

$$\mathcal{D}_1=\mathrm{diag}\left[0,\frac{\gamma_m}{2}(2n_m+1)\right],$$
$$\mathcal{D}_2=\frac{\kappa_1}{2}\begin{bmatrix} M+M^*+2N+1 & \mathrm{i}(M^*-M) \\ \mathrm{i}(M^*-M) & 2N+1-M-M^* \end{bmatrix},$$
$$\mathcal{D}_3=\mathrm{diag}\left[\frac{\kappa_2}{2}(2n_{\mathrm{th}}+1),\frac{\kappa_2}{2}(2n_{\mathrm{th}}+1)\right].$$

The dynamic evolution of quantum fluctuations can be fully captured using the motion equation (16). Next, we will primarily investigate the influence of squeezed vacuum noise on quantum entanglement in optomechanical systems operating under the unresolved-sideband regime, i.e., $\kappa_1>\omega_m$.

4. Bipartite and tripartite entanglement under the unresolved-sideband regime

In this section, we first investigate the enhancement of bipartite entanglement by applying a weak squeezed vacuum field. Since the asymptotic state of the system is Gaussian, we employ logarithmic negativity E_{N}[67,68] as a convenient measure of entanglement,

$$E_{\mathrm{N}}=\max[0,-\ln(2\eta^-)], \tag{17}$$

where the coefficient $\eta^-=\min|\mathrm{i}\Omega_2\tilde{\mathcal{V}}_4|$ with symplectic matrix $\Omega_2=\oplus_{j=1}^{2}\mathrm{i}\sigma_y$. The matrix $\tilde{\mathcal{V}}_4=\mathcal{P}_{1|2}\mathcal{V}_4\mathcal{P}_{1|2}$, where $\mathcal{V}_4$ represents the 4×4 CM of the two subsystems, and $\mathcal{P}_{1|2}$ denotes the partial transposition matrix. For the bipartite entanglement, we investigate the quantum entanglement dynamics between the mechanical mode m and the cavity mode a_2; thus, $\mathcal{V}_4$ can be expressed as

$$\mathcal{V}_4=\begin{bmatrix} \mathcal{V}_m & \mathcal{V}_{cm} \\ \mathcal{V}_{cm}^{\mathrm{T}} & \mathcal{V}_c \end{bmatrix} \tag{18}$$

with $\mathcal{V}_m$, $\mathcal{V}_c$, and $\mathcal{V}_{cm}$ serving as 2×2 subblock matrices.

Furthermore, the quantum feature of the system can also be characterized by tripartite entanglement, which can be achieved via the residual contangle[69,70] and defined as

$$R_\tau^{i|jk}\equiv C_{i|jk}-C_{i|j}-C_{i|k},\quad (i,j,k=m,a_1,a_2), \tag{19}$$

where $C_{u|v}$ refers to the contangle of subsystems of u and v (v contains one or two modes) and is equal to the squared logarithmic negativity, i.e., $C_{u|v}=E_{u|v}^2$. When v contains two modes, $E_{u|v}$ can also be solved using Eq. (17). The specific formulas are as follows: $\eta^-=\min|\mathrm{i}\Omega_3\tilde{\mathcal{V}}_6|$ with $\Omega_3=\oplus_{j=1}^{3}\mathrm{i}\sigma_y$ and $\tilde{\mathcal{V}}_6=\mathcal{P}_{i|jk}\mathcal{V}_6\mathcal{P}_{i|jk}$. Here, $\mathcal{V}_6$ is the 6×6 CM related to the mechanical mode and two cavity modes. Here, the partial transposition matrices are $\mathcal{P}_{m|a_1a_2}=\mathrm{diag}[1,-1,1,1,1,1]$, $\mathcal{P}_{a_1|a_2m}=\mathrm{diag}[1,1,1,-1,1,1]$, and $\mathcal{P}_{a_2|ma_1}=\mathrm{diag}[1,1,1,1,1,-1]$. Regarding the Gaussian nature of the quantum states, the minimal residual contangle is widely acknowledged as a standard measure for the tripartite entanglement

$$R_\tau^{\min}\equiv\min(R_\tau^{m|a_1a_2},R_\tau^{a_1|a_2m},R_\tau^{a_2|ma_1}). \tag{20}$$

Values of $R_\tau^{\min}>0$ imply genuine tripartite entanglement.

To select appropriate parameters to ensure the stability of the optomechanical system, we analyzed the characteristics of the drift matrix $\mathcal{R}(t)$ at the initial time in detail, as displayed in Figs. 3(a) and 3(b). In Fig. 3(a), the maximum real part of the eigenvalues of $\mathcal{R}(t)$ is plotted as a function of the cavity decay rates κ_1 and κ_2, which implies a stable condition associated with the negative value. Figure 3(a) shows that when the decay rate κ_1/ω_m exceeds 2.6, the system enters a stable region covering the entire parameter range. Similarly, Fig. 3(b) demonstrates the dependence of stability on the single-photon coupling strength G_0 and the cavity a_1 detuning δ_1. It suggests that when the value of G_0/ω_m is relatively small, the system also exhibits good stability. These results demonstrate that the proposed scheme is stable over a relatively wide range of parameters. Based on the aforementioned stability analysis, we will further explore the performance of an additional squeezed vacuum field under stable conditions. In Fig. 3(c), we depict the time evolution of bipartite entanglement for the mechanical

mode m and the cavity mode a_2 under different squeezing parameters r. The results indicate that increasing r within an appropriate range leads to a significant enhancement of quantum entanglement, reaching up to 2.76 times the value observed in the absence of the squeezed vacuum field; moreover, after the application of the squeezed vacuum field, the entanglement can easily surpass the strong entanglement limit of ln2 (approximately 0.693). This result emphasizes the significance of utilizing squeezed vacuum fields in optomechanical systems, as they not only facilitate breaking the 0.693 threshold to achieve strong entanglement but also enable precise adjustment of the entanglement effect, resulting in a several-fold enhancement. At the initial moment of evolution, the system is typically in the vacuum state. When the squeezing parameter r is sufficiently large, quantum entanglement is rapidly generated, leading to a transient entanglement peak within a short time interval. Over time, the entanglement gradually approaches a steady state, and the peak correspondingly decays. It is worth noting that although a squeezed vacuum field can effectively suppress quantum noise in one quadrature component, the Heisenberg uncertainty principle dictates that it simultaneously amplifies the noise in the conjugate quadrature. This competition between noise suppression and amplification results in a non-monotonic dependence of entanglement on the squeezing parameter r; consequently, there exists an optimal value of r at which the system achieves maximal entanglement.

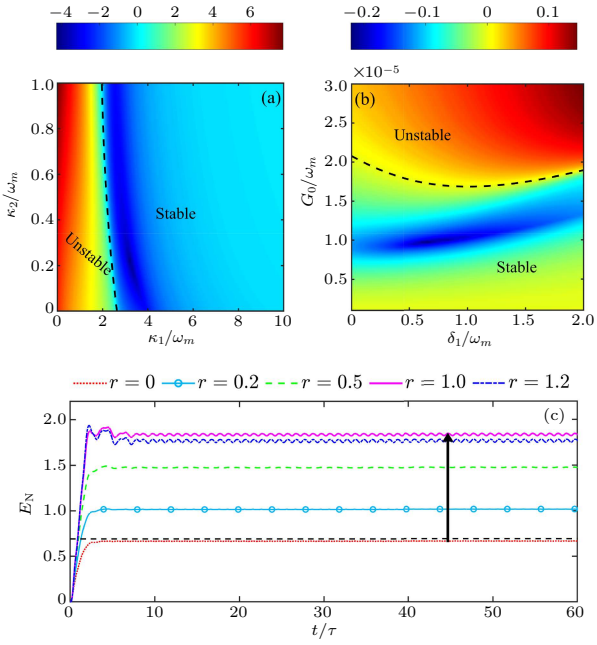


Fig. 3. Steady-state conditions and system dynamics. (a) Maximum eigenvalue of the coefficient matrix $\mathcal{R}$ as a function of the cavity decay rates κ_1 and κ_2. (b) Maximum eigenvalue of the coefficient matrix $\mathcal{R}$ versus the single-photon coupling strength G_0 and the cavity a_1 detuning δ_1. (c) Time evolution of bipartite entanglement E_N between the mechanical oscillator m and the cavity a_2 with respect to the squeezing parameter r. The black dashed line represents an entanglement value of ln2. The system parameters are set to $G_0/\omega_m = 10^{-5}$, $\kappa_2/\omega_m = 0.02$, $J/\omega_m = 1$, $E_0/\omega_m = 1.7 \times 10^5$, $E_{\pm 1}/\omega_m = 10^4$, $n_m = 0$, and $\theta = 1.6\pi$. The other parameters are the same as those used for Fig. 2.

Figure 3(c) also indicates that the entanglement varies periodically with time τ. Therefore, in Fig. 4, we select a fixed time point $t = 60\tau$ for further investigation after the system reaches a stable state, i.e., $E_N^{t'} = E_N$ $(t = 60\tau)$. In Fig. 4(a), we fix the squeezing parameter r and focus on exploring the influence of the reference phase θ and coupling strength J between cavity modes a_1 and a_2 on the properties of bipartite entanglement between the mechanical oscillator m and cavity a_2. The results clearly show that the utilization of the squeezed vacuum field allows for flexible adjustment of the degree of entanglement. It not only enables continuous tuning of the entanglement effect within a specific range but also allows for precise manipulation of the entanglement state by changing the reference phase θ. When the entanglement is zero, the noise precisely disrupts the quantum correlation condition, rendering the entire system a classical mixed state. Conversely, when the entanglement reaches its maximum, the noise transferred from cavity a_1 to cavity a_2 and the mechanical oscillator m is minimized, resulting in the strongest quantum correlation between cavity a_2 and the mechanical oscillator m. It can be seen that the optimal phase for entanglement is not fixed but is jointly determined by the system parameters. Nevertheless, regardless of the specific parameter choices, the phase consistently retains its ability to effectively control the entanglement strength. Notably, the optimization of coupling strength J plays a crucial role in enhancing entanglement: as coupling strength J increases moderately, the mediating effect of a_1 is significantly activated, enabling strong entanglement to emerge between the mechanical oscillator m and cavity a_2, which are originally indirectly coupled, thereby resulting in remarkably enhanced entanglement.

The physical mechanism of entanglement enhancement under the squeezed vacuum field may be explained as follows. Since the squeezed vacuum field is applied to cavity mode a_1, its quantum noise can be effectively restricted; however, the bipartite entanglement between the mechanical oscillator m and cavity a_2 is still limited by standard quantum noise. Meanwhile, the nonclassical noise correlations of cavity a_1 can be transferred to cavity a_2 through the beam-splitter interaction, i.e., $J(a_1^\dagger a_2 + a_1 a_2^\dagger)$, effectively creating a low-noise quantum environment for cavity a_2. This is equivalent to previously purifying the environment of cavity a_2, thereby making it easier to generate strong entanglement (such as bipartite or tripartite entanglement). Because cavity a_1 has already provided nonclassical resources, cavity a_2 can utilize them directly, achieving strong enhancement of entanglement. Therefore, by combining the dynamic control capability of the squeezed vacuum field with the adjustable coupling characteristics of the dual-cavity system, we can precisely manipulate the generation of entanglement.

To further clarify the role of the squeezed vacuum field in

a thermally noisy environment, Fig. 4(b) focuses on the variation of entanglement between mechanical mode m and cavity mode a_2 with respect to the squeezing parameter r and the thermal environmental temperature T. An obvious trend can be observed: as the environmental temperature T increases, systems with a larger squeezing parameter r exhibit slower entanglement reduction. This directly demonstrates that the squeezed vacuum field can effectively enhance the robustness of entanglement against thermal noise; the greater the value of the squeezing parameter r, the more pronounced this noise-resistance capability becomes.

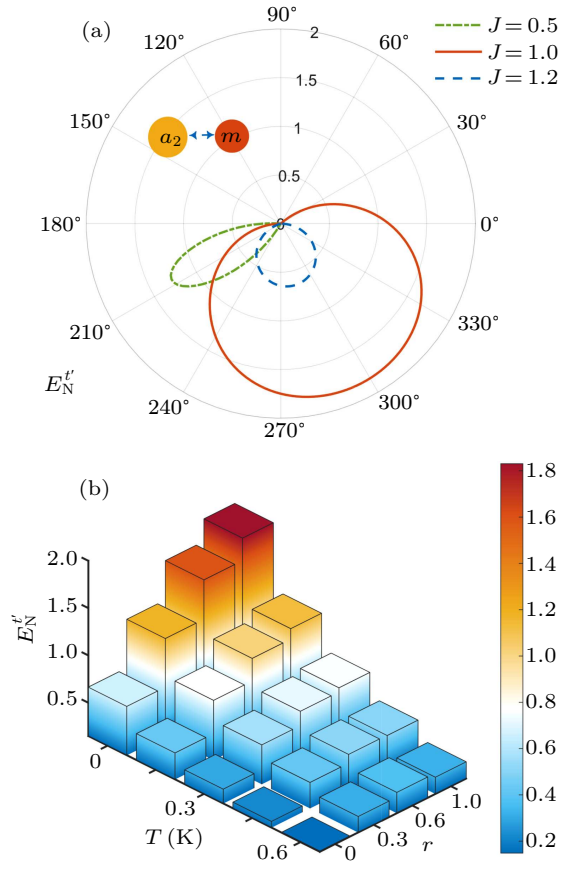


Fig. 4. (a) Variation of logarithmic negativity $E_{\mathrm{N}}^{t'}$ with phase θ in polar coordinates for coupling strength J values of 0.5, 1.0, and 1.2. (b) Three-dimensional bar plot illustrating the variation of $E_{\mathrm{N}}^{t'}$ as a function of temperature T and squeezing parameter r. The other parameters are consistent with those in Fig. 3.

Progressing from bipartite entanglement to the more complex tripartite entanglement, Fig. 5(a) examines the impact of the squeezed vacuum field on the time evolution of tripartite entanglement. By comparing the two scenarios (with and without the squeezed vacuum field), it can be intuitively observed that after the squeezed vacuum field is applied, the minimum value of the tripartite entanglement evolution reaches 2.24 times that of the case without the squeezed vacuum field, while the maximum value reaches 1.52 times that of the case without it. Owing to the constructive interference arising from phase matching between the squeezed vacuum field and the modulation light field, the quantum entanglement in the system is significantly enhanced. Moreover, in the absence of the squeezed vacuum field, the entanglement exhibits a simple single-frequency oscillation. When the field is applied, the dynamics become significantly more complex, deviating from pure sinusoidal behavior, and the oscillation amplitude after stabilization is markedly reduced. This result not only demonstrates that the squeezed vacuum field enhances the entanglement effect but also reveals its unique advantage in improving the stability of entanglement. Furthermore, the inset magnification from $t/\tau = 57$ to $t/\tau = 60$ provides additional evidence that the analytical solution of the first moments (squares and circles) we derived agrees very well with the numerical solution (solid and dashed lines). As can be clearly seen from Fig. 5(a), the minimal residual contangle $R_{\tau}^{\min}$ varies periodically with τ, and we will fix the time at $t = 60\tau$ for subsequent analysis, $R_{\tau,t'}^{\min} = R_{\tau}^{\min}\ (t = 60\tau)$.

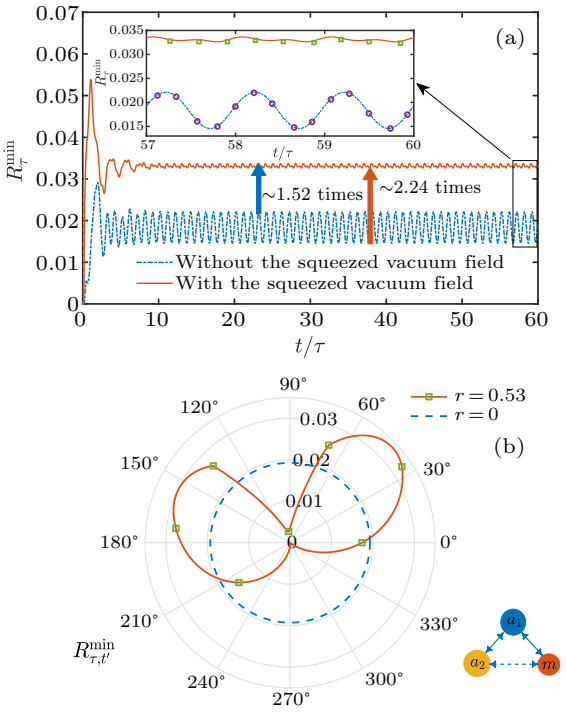


Fig. 5. (a) The dynamics of tripartite entanglement $R_{\tau}^{\min}$ as a function of time in the presence and absence of the squeezed vacuum field. The square and circular markers in the inset enlargement represent the tripartite entanglement images plotted for analytical solutions of $\langle q(t)\rangle$ and $\langle a_1(t)\rangle$. (b) The tripartite entanglement $R_{\tau,t'}^{\min}$ versus θ in polar coordinates. The squeezing parameter is set to $r = 0.53$, and the reference phase is set to $\theta = 0.26\pi$. The other parameters are the same as those used for Fig. 4.

Further analysis of the results in Fig. 5(b) provides additional evidence for the regulatory role of the squeezed vacuum field on entanglement from another perspective. By comparing the scenarios with and without the squeezed vacuum field, it is found that, similar to the regulatory behavior of bipartite entanglement in Fig. 4(a), the degree of tripartite entanglement can be arbitrarily adjusted over a full 2π period by varying the reference phase, θ. This further stresses the significance of the reference phase in manipulating entanglement.

To systematically reveal the synergistic effects of the squeezed vacuum field and coupling strength J on tripartite entanglement, we fix the reference phase θ in Fig. 6(a) and focus on examining the influence of the squeezing parameter r and coupling strength J. The results show that the introduction of the squeezed vacuum field still allows the entanglement to be tuned within a specific range, allowing flexible control over the entanglement strength by adjusting the value of the squeezing parameter, r. Meanwhile, the optimization of the coupling strength J is equally critical. Given the beam–splitter interaction between cavity a_1 and cavity a_2, appropriately enhancing their mutual interaction can effectively strengthen the mediating role of cavity a_1, enabling the quantum noise of both cavity modes a_1 and a_2 to be effectively reduced, thereby significantly elevating the overall level of tripartite entanglement.

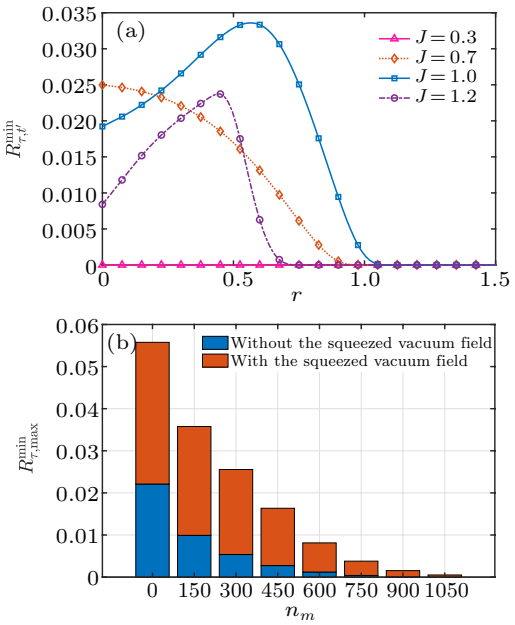


Fig. 6. (a) The variation of tripartite entanglement $R^{\min}_{\tau,t'}$ with squeezing parameter r for different coupling strengths J. (b) A comparison of $R^{\min}_{\tau,\max}$ as a function of the average thermal phonon number n_m in the presence and absence of the squeezed vacuum field. The blue bars represent the scenario without the squeezed vacuum field, while the orange bars depict the case with the squeezed vacuum field. For the system parameters, refer to Fig. 5.

In Fig. 6(b), we use bar charts (blue areas for the case without the squeezed vacuum field, orange areas for the case with the squeezed vacuum field) to visually illustrate the variation of the maximum tripartite entanglement with the average thermal phonon number n_m. The formula for the maximum value of tripartite entanglement is $R^{\min}_{\tau,\max} = \max[R^{\min}_{\tau}(t)]$. The data clearly indicate that after the squeezed vacuum field is applied, the degree of tripartite entanglement increases many times compared to the case without the squeezed field, regardless of how much the average thermal phonon number n_m increases. Moreover, the trend of enhanced noise resistance is even more pronounced. From the perspective of noisy environments, this result once again verifies the superiority of the squeezed vacuum field in enhancing entanglement stability and robustness against interference.

5. Conclusions

In conclusion, we have investigated the entanglement behavior in a coupled optomechanical system under the unresolved-sideband regime driven by an amplitude-modulated laser field and a weak squeezed vacuum field. By adjusting the squeezed vacuum field and the coupling strength between the two cavities, substantial bipartite entanglement and several-fold enhanced tripartite entanglement are achieved. Moreover, the introduction of the squeezed vacuum field is of great significance for entanglement control, enabling continuous and precise manipulation of entanglement within specific ranges. To clarify the mechanism of the squeezed vacuum field, this study comparatively analyzes the variations in bipartite and tripartite entanglement with and without the squeezed vacuum field, while also exploring the impact of thermal noise on entanglement characteristics. The results demonstrate that applying the squeezed vacuum field not only significantly enhances the system's entanglement performance but also substantially improves its robustness. Our work offers a novel and experimentally realizable approach to achieving strong bipartite and tripartite entanglement, while also providing new insights for developing more resilient quantum technologies.

Acknowledgements

This work was supported by the National Natural Science Foundation of China (Grant Nos. 12204440 and 12404418), the China Postdoctoral Science Foundation (Grant No. 2025M773357), and the Fundamental Research Program of Shanxi Province, China (Grant No. 202303021212171).

References

[1] Kippenberg T J and Vahala K J 2008 *Science* **321** 1172
[2] Favero I and Karrai K 2009 *Nat. Photonics* **3** 201
[3] Aspelmeyer M, Kippenberg T J and Marquardt F 2014 *Rev. Mod. Phys.* **86** 1391
[4] Imamoğlu A, Schmidt H, Woods G and Deutsch M 1997 *Phys. Rev. Lett.* **79** 1467
[5] Xia K, Nori F and Xiao M 2018 *Phys. Rev. Lett.* **121** 203602
[6] Dong Y, Zheng X, Wang D and Zhao P 2025 *Chin. Phys. B* **34** 044203
[7] Man X X, Sun J, Zhang W Z, Luo L and Jin G 2024 *Chin. Phys. B* **33** 120303
[8] Ashkin A 1980 *Science* **210** 1081
[9] Bai C H, Wang D Y, Zhang S, Liu S and Wang H F 2019 *Ann. Phys.* **531** 1800271
[10] Einstein A, Podolsky B and Rosen N 1935 *Phys. Rev.* **47** 777
[11] Schrödinger E 1935 *Math. Proc. Cambridge Philos. Soc.* **31** 555
[12] Dong L H, Wu X J, Bai C H and Wu S X 2025 *Chin. Phys. B* **34** 020304
[13] Vitali D, Gigan S, Ferreira A, Böhm H R, Tombesi P, Guerreiro A, Vedral V, Zeilinger A and Aspelmeyer M 2007 *Phys. Rev. Lett.* **98** 030405
[14] Chen P, Luo D W and Yu T 2025 *Phys. Rev. Research* **7** 013161
[15] Wu S X, Bai C H, Li G, Yu C S and Zhang T 2024 *Opt. Express* **32** 260
[16] Yang W Q, Leng X, Cheng J and Zhang W Z 2024 *Chin. Phys. B* **33** 060313

[17] Liu M Y, Gong Y, Chen J, Wang Y W and Xiong W 2025 *Chin. Phys. B* **34** 057202
[18] Zhou B Y, Pan N, Yu L and Li G X 2024 *Phys. Rev. A* **110** 032401
[19] Yang J, Zhao C, Wang D W, Peng R and Zhou L 2024 *Phys. Rev. Appl.* **21** 044056
[20] Wu S X, Bai C H, Li G, Yu C S and Zhang T 2023 *J. Opt. Soc. Am. B* **40** 2885
[21] Li R, Long Y and Zhang X 2025 *Chin. Phys. B* **34** 020307
[22] Asjad M, Agarwal G S, Kim M S, Tombesi P, Giuseppe G Di and Vitali D 2014 *Phys. Rev. A* **89** 023849
[23] Tong J L, Hao Y, Wu S X, Bai C H and Bai S 2025 *Adv. Quantum Technol.* **8** 2400654
[24] Agarwal G S and Huang S 2016 *Phys. Rev. A* **93** 043844
[25] Wu X J, Cheng H H, Wu Q, Bai C H and Wu S X 2024 *Opt. Express* **32** 35663
[26] Chen S S, Xie Y L, Zhang J J, Zhang N N, Guo Y R, Yang H and Ma Y 2025 *Chin. Phys. B* **34** 014201
[27] Birnbaum K M, Boca A, Miller R, Boozer A D, Northup T E and Kimble H J 2005 *Nature* **436** 87
[28] Luo Y, Zhang X, Xiao Y, Xu J, Li H, Yang Y and Xia X 2025 *Chin. Phys. B* **34** 014203
[29] Gao X C, Wu X J, Bai C H, Wu S X and Yu C S 2023 *Opt. Express* **31** 36796
[30] Rabl P 2011 *Phys. Rev. Lett.* **107** 063601
[31] Huang R, Miranowicz A, Liao J Q, Nori F and Jing H 2018 *Phys. Rev. Lett.* **121** 153601
[32] Wu S X, Gao X C, Cheng H H and Bai C H 2025 *Phys. Rev. A* **111** 043714
[33] Metelmann A and Clerk A A 2015 *Phys. Rev. X* **5** 021025
[34] Qian Y B, Zhang Z Y, Tang L, Lai D G and Hou B P 2024 *Phys. Rev. A* **109** 043103
[35] Vinokur V M, Baturina T I, Fistul M V, Mironov A Y, Baklanov M R and Strunk C 2008 *Nature* **452** 613
[36] Zhirov O V and Shepelyansky D L 2006 *Eur. Phys. J. D* **38** 375
[37] Liao C G, Chen R X, Xie H, He M Y and Lin X M 2019 *Phys. Rev. A* **99** 033818
[38] Vaidya G M, Jäger S B and Shankar A 2025 *Phys. Rev. A* **111** 012410
[39] Lai D G, Qin W, Hou B P, Miranowicz A and Nori F 2021 *Phys. Rev. A* **104** 043521
[40] Qiu J, Jin L J, Peng Z Y, Chesi S and Wang Y D 2022 *Phys. Rev. A* **105** 033514
[41] Shao W, Li J and Wang L L 2023 *Phys. Rev. A* **107** 063505
[42] Clarke J, Neveu P, Khosla K E, Verhagen E and Vanner M R 2023 *Phys. Rev. Lett.* **131** 053601
[43] Li J, Zhu S Y and Agarwal G S 2018 *Phys. Rev. Lett.* **121** 203601
[44] Guo Y, Zhao J, Cao L, Li Y and Lu H Y 2025 *Chin. Phys. B* **34** 024203
[45] Yang J, Lu T X, Peng M, Liu J, Jiao Y F and Jing H 2024 *Opt. Express* **32** 785
[46] Hei X L, Li P B, Pan X F and Nori F 2023 *Phys. Rev. Lett.* **130** 073602
[47] Zheng Q, Cao Y and Yan P 2025 *Chin. Phys. B* **34** 107514
[48] Chen J, Fan X G, Xiong W, Wang D and Ye L 2024 *Phys. Rev. A* **109** 043512
[49] Din G, Abbas M and Zhang P 2024 *Eur. Phys. J. Plus* **139** 591
[50] Ghosh J, Mondal S, Varshney S K and Debnath K 2024 *Phys. Rev. A* **109** 023512
[51] Yang Z, Xiong B, Zhao C and Zhou L 2025 *Opt. Express* **33** 5123
[52] Dilawaiz, Qamar S and Irfan M 2024 *Phys. Rev. A* **109** 043708
[53] Hussain B, Qamar S and Irfan M 2022 *Phys. Rev. A* **105** 063704
[54] Wang Y, Wu J L, Jiao Y F, Lu T X, Zhang H L, Jiang L Y, Kuang L M and Jing H 2025 *Phys. Rev. A* **111** 013709
[55] Feng J S, Tan L, Gu H Q and Liu W M 2017 *Phys. Rev. A* **96** 063818
[56] Liu Z Q, Liu J, Tan L and Liu W M 2024 *Phys. Rev. A* **110** 023707
[57] Zhang W J, Zhang Y, Guo Q, Liu A P, Li G and Zhang T 2021 *Phys. Rev. A* **104** 053506
[58] Chakraborty S and Sarma A K 2018 *Phys. Rev. A* **97** 022336
[59] Mari A and Eisert J 2009 *Phys. Rev. Lett.* **103** 213603
[60] Liu Y C, Xiao Y F, Jiang X F, Li B B, Li Y and Gong Q 2012 *Phys. Rev. A* **85** 013843
[61] Sedlmeir F, Foreman M R, Vogl U, Zeltner R, Schunk G, Strekalov D V, Marquardt C, Leuchs G and Schwefel H G 2017 *Phys. Rev. Appl.* **7** 024029
[62] Trainor L S, Sedlmeir F, Peuntinger C and Schwefel H G 2018 *Phys. Rev. Appl.* **9** 024007
[63] Singh V, Shevchuk O, Blanter Y M and Steele G A 2016 *Phys. Rev. B* **93** 245407
[64] Hochreiter A, Bredol P, David F, Demiralp B, Weber H B and Weig E M 2025 *Phys. Rev. Appl.* **24** 034005
[65] Kono S, Masuyama Y, Ishikawa T, Tabuchi Y, Yamazaki R, Usami K, Koshino K and Nakamura Y 2017 *Phys. Rev. Lett.* **119** 023602
[66] Bienfait A, Campagne-Ibarcq P, Kiilerich A H, Zhou X, Probst S, Pla J J, Schenkel T, Vion D, Esteve D, Morton J J L, Moelmer K and Bertet P 2017 *Phys. Rev. X* **7** 041011
[67] Vidal G and Werner R F 2002 *Phys. Rev. A* **65** 032314
[68] Plenio M B 2005 *Phys. Rev. Lett.* **95** 090503
[69] Adesso G and Illuminati F 2006 *New J. Phys.* **8** 15
[70] Adesso G and Illuminati F 2007 *J. Phys. A: Math. Theor.* **40** 7821